Covalently Assembled NIR Nanoplatform for Simultaneous Fluorescence Imaging and Photodynamic Therapy of Cancer Cells

12 AUTHORS, INCLUDING:

Kai Liu
University of Amsterdam
14 PUBLICATIONS **307** CITATIONS

Qinghui Zeng
Changchun Institute of Optics, Fine Mechani…
49 PUBLICATIONS **733** CITATIONS

Saskia A G Lambrechts
Janssen Biologics
21 PUBLICATIONS **518** CITATIONS

M.C.G Aalders
University of Amsterdam
125 PUBLICATIONS **2,434** CITATIONS

Covalently Assembled NIR Nanoplatform for Simultaneous Fluorescence Imaging and Photodynamic Therapy of Cancer Cells

Kai Liu,[†,‡,§,⊥] Xiaomin Liu,[†] Qinghui Zeng,[†] Youlin Zhang,[†] Langping Tu,[†] Tao Liu,[†] Xianggui Kong,[†,*] Yinghui Wang,[§] Feng Cao,[§] Saskia A. G. Lambrechts,[⊥] Maurice C. G. Aalders,[⊥,*] and Hong Zhang[§,*]

[†]State Key Laboratory of Luminescence and Applications, Changchun Institute of Optics, Fine Mechanics and Physics, Chinese Academy of Sciences, Changchun 130033, People's Republic of China, [‡]Graduate School of Chinese Academy of Sciences, Beijing 100039, People's Republic of China, [§]Van't Hoff Institute for Molecular Sciences, University of Amsterdam, Science Park 904, 1098 XH Amsterdam, The Netherlands, and [⊥]Department of Biomedical Engineering and Physics, Academic Medical Center, University of Amsterdam, 1105 AZ Amsterdam, P.O. Box 22700, The Netherlands

Photodynamic therapy (PDT) is an emerging therapeutic modality using photosensitizers (PS) and light irradiation to eradicate cancer tissues. Under proper light excitation, on one hand, the PS can interact with molecular oxygen and generate cytotoxic singlet oxygen ($^1O_2$, type II) for killing cancer cells;[1−4] on the other hand the inherent photoluminescence from PS can also be used for fluorescence imaging and localizing the diseases, which is often referred to as photodynamic diagnosis (PDD).[4−7] However, phototriggered theranostics[6] based on traditional photosensitizing molecules suffer mainly from low signal-to-noise ratio (SNR), small tissue penetration depth, and photobleaching of PS. In addition, two different wavelength lights are always adopted to implement respectively imaging and therapy, which makes it difficult for real-time monitoring and evaluating PDT efficacy. For example for 5-ALA administrated theranosis, excitation at 405 nm is adopted for PDD, whereas 630 nm irradiation is applied for PDT. The contradictory requirements of high $^1O_2$ production for PDT and strong fluorescence for PDD make it difficult to realize simultaneous imaging and therapy employing existing photosensitizers. Therefore it is very appealing to create new photosensitizing nanoplatforms that can simultaneously perform on-site fluorescence imaging and photodynamic therapy under a single-light irradiation.

Recently, lanthanide ion (Ln³⁺, such as Er³⁺, Tm³⁺, Ho³⁺)-doped upconversion nanoparticles (UCNPs) have received much attention in biomedicine.[8−33] Because of the unique ladder-like energy level structures of

ABSTRACT
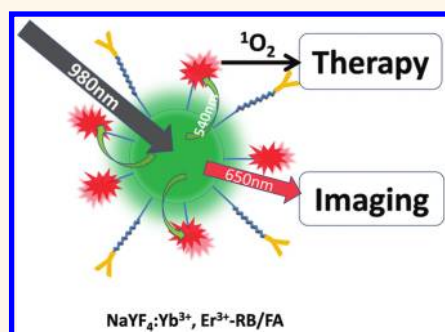
A highly efficient multifunctional nanoplatform for simultaneous upconversion luminescence (UCL) imaging and photodynamic therapy has been developed on the basis of selective energy transfer from multicolor luminescent NaYF$_4$:Yb³⁺,Er³⁺ upconversion nanoparticles (UCNPs) to photosensitizers (PS). Different from popular approaches based on electrostatic or hydrophobic interactions, over 100 photosensitizing molecules were covalently bonded to every 20 nm UCNP, which significantly strengthened the UCNP—PS linkage and reduced the probability of leakage/desorption of the PS. Over 80% UCL was transferred to PS, and the singlet oxygen production was readily detected by its feature emission at 1270 nm. Tests performed on JAR choriocarcinoma and NIH 3T3 fibroblast cells verified the efficient endocytosis and photodynamic effect of the nanoplatform with 980 nm irradiation specific to JAR cancer cells. Our work highlights the promise of using UCNPs for potential image-guided cancer photodynamic therapy.

KEYWORDS: upconversion nanoparticles · covalent bonding · energy transfer · singlet oxygen · fluorescence imaging · photodynamic therapy

Ln³⁺, UCNPs are able to convert NIR to visible lights efficiently.[34,35] Their application in fluorescence imaging has shown various benefits, including significantly improved tissue penetration depth, large Stokes shift, reduced autofluorescence, and enhanced photostability.
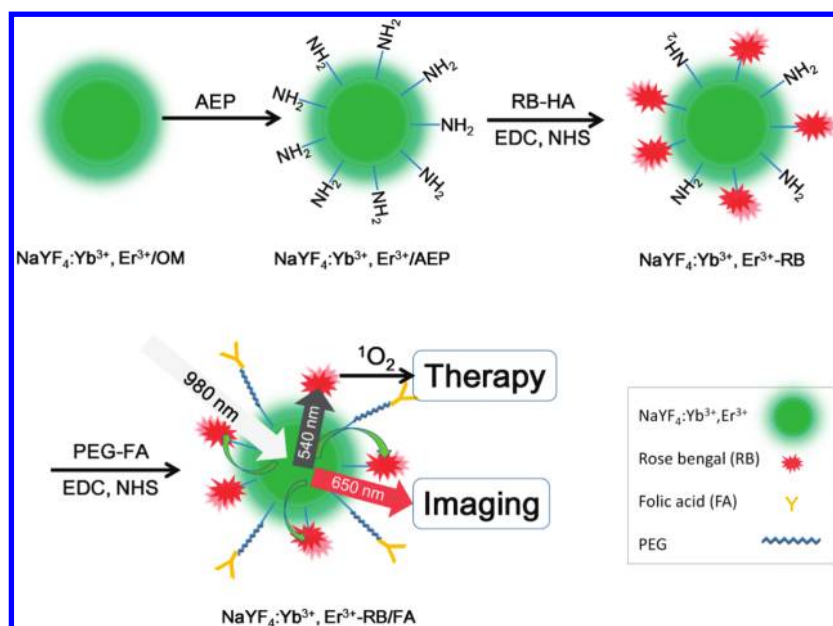
Scheme 1. Covalent conjugation of NaYF$_4$:Yb^{3+},Er^{3+} UCNPs, photosensitizer RB, and target molecule FA.

Up to now, several approaches have been reported in developing PDT reagents based on UCNPs, such as silica encapsulation,[27−29] polymer encapsulation,[30,31] and hydrophobic interaction.[32,33] Cytotoxic singlet oxygen is generated through photosensitizing molecules that are activated *via* an energy transfer process from excited UCNPs, wherein UCNPs play a role of energy transducer for NIR light. Production of $^1O_2$ is obviously dependent on the energy transfer efficiency which relies on the spectral overlap between the donor and acceptor, the distance between the two, and the amount of photosensitizing molecules loaded on each UCNP. However, PS loading efficiency of these noncovalently formed UCNP−PS complexes is usually low. For example, it was reported that following the hydrophobic interaction approach only about 5 Zn-PC molecules were linked to a 50 nm NaYF$_4$:Yb^{3+},Er^{3+} nanoparticle, which was much less than the number of donors (emission centers).[33] In addition, the desorption and/or leakage of PS from the nanoplatform is also a big concern. In a recent report,[30] although a large number of meso-tetraphenylporphine (TPP, 10 wt %) photosensitizers were originally colocalized within PEG layer-functionalized NaYF$_4$:Yb^{3+},Er^{3+} UCNPs *via* a flash nanoprecipitation (FNP) coating method, high excitation power density (>100 W/cm^2) was, however, still necessary in order to receive an observable therapeutic effect, which indicated low singlet oxygen production. This phenomenon might be related with the poor stability of the originally loaded photosensitizers in UCNPs. In general, noncovalent adsorption is not an ideal approach in uploading photosensitizing molecules for energy-transfer-based PDT/PDD.

To meet the demands of high fluorescent intensity and high $^1O_2$ production yield, we have in this work developed a multifunctional upconversion nanoplatform for simultaneous imaging and therapy. Upon NIR continuous wave (CW) laser excitation, two upconversion luminescence bands of NaYF$_4$:Yb^{3+},Er^{3+}, peaking around 540 and 650 nm, are employed for simultaneous PDT and PDD, respectively (Scheme 1). As mentioned above, high PS loading is necessary to achieve high energy transfer efficiency and subsequent high singlet oxygen production. For that, a covalent conjugating strategy is adopted to link functionalized UCNPs with the photosensitizing molecule Rose Bengal (RB). Under 980 nm excitation the singlet oxygen is readily detected *via* its feature emission at 1270 nm. To the best of our knowledge, this is the first time that $^1O_2$ from upconversion nanoplatforms is directly probed. Relevant *in vitro* experiments on cancer and noncancerous cells are performed to validate the design of the novel upconversion nanoplatform.

RESULTS AND DISCUSSION

Characterization of Amino-Functionalized NaYF$_4$:Yb^{3+},Er^{3+} UCNPs. The hydrophilic UCNPs of NH$_2$-functionalized NaYF$_4$:Yb^{3+},Er^{3+} were prepared *via* a ligand exchanging process using 2-aminoethyl dihydrogen phosphate (AEP) as surface coating agent to replace the original oleylamine (OM) ligands. The crystal structures and the phase purity of the NaYF$_4$:Yb^{3+},Er^{3+} UCNPs were examined by XRD, as presented in Figure S1 in the Supporting Information. The diffraction peaks of the UCNPs are well-defined, and the peak positions and intensities agree well with the standard pattern of hexagonal NaYF$_4$ (line pattern in Figure S1, JCPDS No. 16-0334), confirming the high quality of the samples. The average size of the NaYF$_4$:Yb^{3+},Er^{3+} UCNPs is determined to be ∼20 nm in diameter from TEM measurements (Figure 1), consistent with the XRD
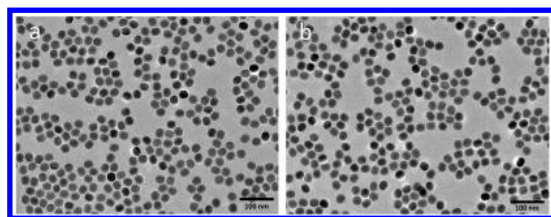
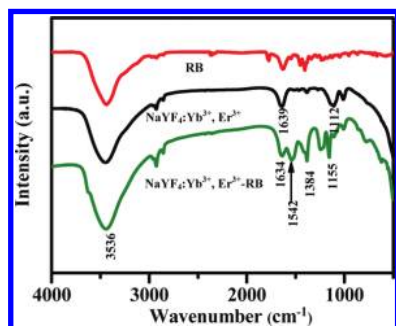**Figure 1.** TEM images of OM- or AEP-stabilized $NaYF_4:Yb^{3+}$, Er^{3+} nanoparticles (scale bar: 100 nm).

Figure 2. FTIR absorption spectra of amino-functionalized RB (red curve), $NaYF4:Yb^{3+},Er^{3+}$ UCNPs (black curve), and UCNPs—PS nanoconjugates (green curve).

Figure 3. Absorption spectra of RB eluate after washing with DMSO 1, 2, and 3 times the physically adsorbed $NaYF_4$: Yb^{3+},Er^{3+}—RB complexes (solid lines) and the covalently bonded $NaYF_4:Yb^{3+},Er^{3+}$—RB nanoconjugates (dashed lines, see also inset).

results. Figure 1 also demonstrates the high monodispersity of the nanoparticles.

FTIR absorption spectra (Figure S2a) confirm that AEP molecules were coated on the surface of UCNPs. Upconversion luminescence spectra of OM- or AEP-stabilized UCNPs (Figure S2b) show little difference, which indicates that the ligand exchange process had a negligible effect on the optical properties of UCNPs. The amino-functioned $NaYF_4:Yb^{3+},Er^{3+}$ nanoparticles were stabilized in water for seven days without noticeable deposition due to the fact that the phosphate group of AEP molecules can easily form a bidentate bond with the unsaturated rare earth ion at the surface.[36]

Covalent Construction of UCNPs—PS Nanoplatform. As schematically illustrated in Scheme 1, a covalent conjugation strategy was realized via a carbodiimide crosslinking reaction between the amino group of $NaYF_4$: Yb^{3+},Er^{3+} UCNPs and the carboxyl group of hexanoic acid ester of rose bengal (RB-HA). The covalent coupling between UCNPs and RB was confirmed from FTIR absorption spectra in Figure 2. For a free RB-HA the C=O stretching vibration mode of the carboxyl group is located at 1774 cm^{-1}. After conjugating with UCNPs this peak disappeared and two new peaks appeared at 1542 and 1384 cm^{-1}, corresponding to the amide II band of the N—H bending vibration and the amide III band of the C—N stretching vibration, respectively. The absorption peak at 1634 cm^{-1} is partly associated with the C=O stretching vibration from the amide I band.

Owning to the robust covalent bonding between RB and $NaYF_4:Yb^{3+},Er^{3+}$, we could bind around 100 photosensitizing molecules to each UCNP. In principle it could be even higher, but in our case a drawback of
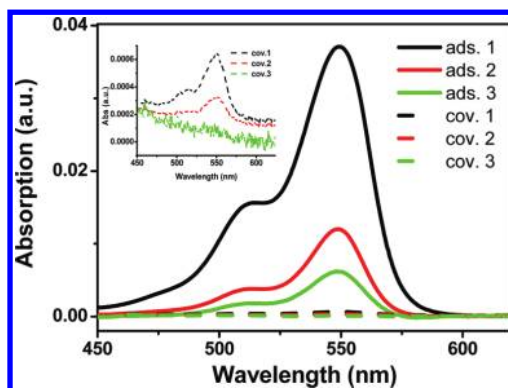
doing so was that the dimerization of RB would become serious, as indicated from the absorption spectra in Figure S3. The relative intensity of the shoulder at short wavelength, corresponding to the dimer absorption, enhances with increasing RB concentration, distinct evidence of the formation of dimers. Figure S4 is the corresponding singlet oxygen production determined by the chemical probe 1,3-diphenylisobenzofuran (DPBF), from which the optimal number of RB for individual $NaYF_4:Yb^{3+},Er^{3+}$ nanoparticles is determined to be ~100. This is in agreement with an earlier report that $^1O_2$ production markedly decreases with the photosensitizer agglomerating process.[37] Compared to popular noncovalent bonding approaches such as electrostatic interactions, covalent bonding is supposed to be very robust, which is in line with our results shown in Figure 3, where the RB eluate after each washing with DMSO was characterized by UV/vis absorption. The spectra tell us that, contrary to obvious RB desorption from electrostatically assembled UCNPs—PS complexes, the amount of RB in the eluate is 1 order of magnitude less for covalently bonded UCNPs—PS conjugates.

Selective Energy Transfer from UCNPs to PS. The multifunctional nanoplatform is constructed on the basis of the selective energy transfer from multicolor upconversion luminescent $NaYF_4:Yb^{3+},Er^{3+}$ UCNPs to photosensitizers. Selective energy transfer can be achieved by properly choosing PS of which the absorption matches a desired upconversion luminescence band of $NaYF_4:Yb^{3+},Er^{3+}$ UCNPs. In this study, a watersoluble photosensitizing molecule, RB, was chosen because its absorption spectrum overlaps perfectly with the green upconversion luminescence (UCL) band (540 nm) of $NaYF_4:Yb^{3+},Er^{3+}$ (Figure 4a). Moreover, RB is a very efficient photosensitizer in producing singlet oxygen.[38]

The selective energy transfer from $NaYF_4:Yb^{3+},Er^{3+}$ to RB is confirmed from both steady-state UCL spectra and luminescent decay lifetimes. The UCL spectra of

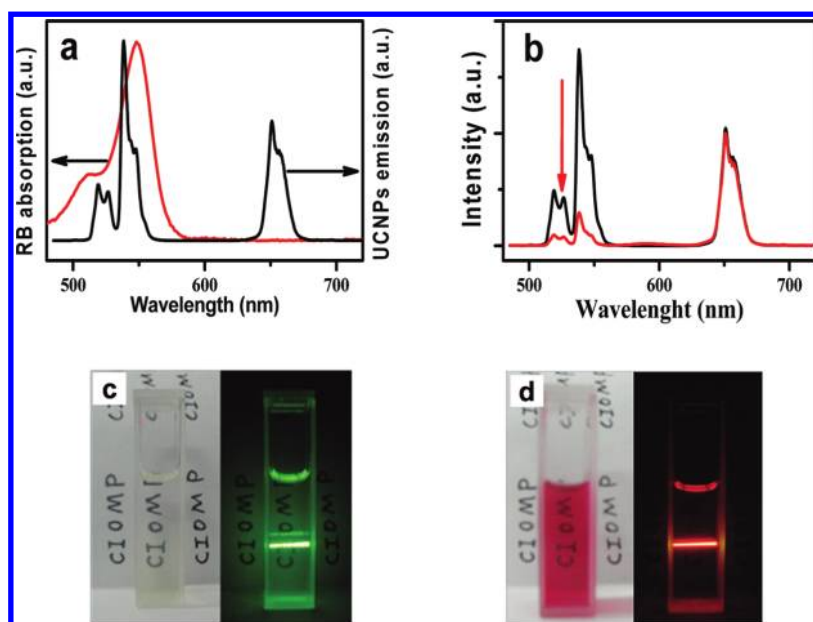Figure 4. (a) Spectral overlap between the upconversion emission spectrum of the donor NaYF$_4$:Yb^{3+},Er^{3+} (black curve) and the absorption spectrum of the acceptor RB (red curve). (b) Upconversion luminescence spectra of UCNPs (black curve) and NaYF$_4$:Yb^{3+},Er^{3+}−RB conjugates (red curve). Photographs of UCNPs (c) and NaYF$_4$:Yb^{3+},Er^{3+}−RB nanoconjugates (d) under ambient light (left) and under 980 nm diode laser irradiation (right).
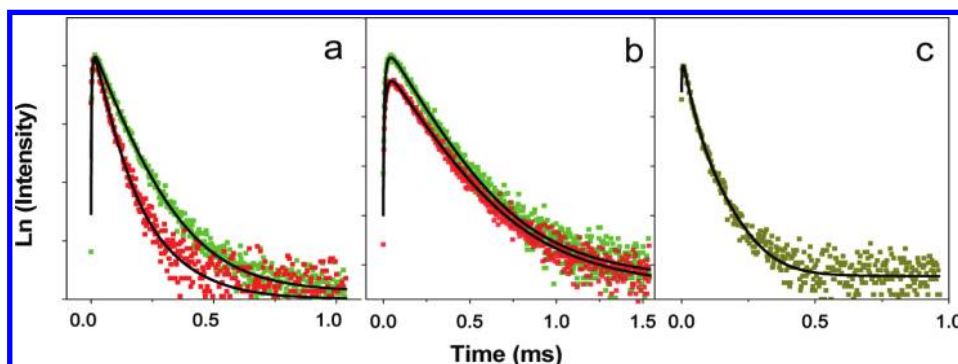

Figure 5. Luminescence decay curves of upconversion emissions monitored (a) at 540 nm, (b) at 650 nm with (in red), and without (in green) photosensitizers. RB fluorescence decay was monitored at 587 nm (c). Best fitting curves are also shown as a solid line.

Figure 4b demonstrate evidently that the 540 nm band was strongly quenched by RB, while the 650 nm band was not. This can be visualized from the obvious fluorescent color changes of the pure UCNPs and the UCNPs−PS conjugates, as given in Figure 4c and d, respectively. Under excitation of 980 nm CW diode laser, UCNPs appeared green (Figure 4c, right), while UCNPs−PS nanoconjugates became red (Figure 4d, right). The fluorescence resonance energy transfer (FRET) efficiency can be estimated from the quenching of green UCL: $E = (I_0 - I_1)/I_0$, where I_0 and I_1 are green emission intensities of free UCNPs and UCNPs−PS nanoconjugates, respectively.[39,40] On the basis of this formula, the energy transfer efficiency was determined as high as 83% for the present covalently bonded nanoconjugates. The high energy transfer efficiency is attributed to the small size of AEP molecules used here for covalent cross-linking photosensitizers, which

shortened the distance between UCNPs and PS compared with the previous reported protocols such as the silica shell encapsulating method, which promoted significantly the energy transfer process.

To further study the energy transfer process from NaYF$_4$:Yb^{3+},Er^{3+} to RB, the temporal behavior of upconversion luminescence of both UPNPs and UCNPs−PS conjugates was recorded at 540 and 650 nm (Figure 5a and b). In both cases the green and the red decay curves could be well fitted with a biexponential function, and the fitted time constants are listed in Table 1. In the presence of photosensitizer RB, the average decay time at 540 nm decreases from 93.34 μs to 55.41 μs, while the average decay time at 650 nm hardly shows any change (from 194.35 μs to 192.65 μs). This is a confirmation of the high selectivity in energy transfer mechanism. Moreover, different from the direct excitation situation, i.e., excitation at

540 nm, where the fluorescence of RB exhibits an exponential decay on the order of nanoseconds, the fluorescent decay lifetime of RB lengthens to 43.70 μs when excited at 980 nm (Figure 5c), which further assures that FRET occurred in the UCNPs—PS conjugates. However, the average lifetime of RB is shorter than that of the donor; that is, the decay of the 540 nm upconversion emission is around 55.41 μs. This discrepancy can be understood from the structure of the UCNPs. In a UCNP there are discrete luminescent centers distributed over the whole nanoparticle, and the distances between these centers to the surface-linked RB are therefore diverse. For those closer to the RB FRET would be more efficient than those further away from RB. Some centers may even be out of the FRET interaction distance and will not participate in the energy transfer. For an efficient FRET the emission time behaviors of the donor and the acceptor would be the same. Considering the distribution of energy donors in an UCNP, the fluorescence kinetics of the acceptor is therefore faster than that of the UCNPs because the UCNP in the present case is an ensemble of luminescent centers of different kinetics.

Singlet Oxygen Production from UCNPs—PS Nanoconjugates. As shown in Figure 6a, the absorption intensity of DPBF monitored at 420 nm decreases exponentially with 980 nm irradiation time when incubated with UCNPs—PS nanoconjugates. In control experiments of (i) DPBF incubated with UCNPs—PS nanoconjugates without 980 nm irradiation and (ii) DPBF incubated

with UCNPs (without loading photosensitizers) and 980 nm irradiation, the absorption of DPBF remains unchanged. This observation illustrates that singlet oxygen could be generated only from the cooperation of UCNPs and the photosensitizer *via* an efficient energy transfer process. After 16 min irradiation 50% of the DPBF was consumed, which was very efficient compared with those shelled with silica, where only 3% of the $^1O_2$ probes was consumed after 16 min of continuous irradiation.[27] In that case both the low photosensitizer uploading efficiency in a nonporous silica shell and the silica shell itself might hamper the encapsulated PS from interacting with molecular oxygen dissolved in solution.[41] In the present UCNPs—PS conjugates covalent bonding between the UCNPs and PS surmounted these shortages because the photosensitizer molecules were bonded firmly with the UNCPs and linked to the terminal side of UCNPs so that the interaction with oxygen was sufficient.

A more direct way to detect singlet oxygen is monitoring its characteristic phosphorescence at 1270 nm, which is usually difficult because of its short lifetime in solution and the limited amount of $^1O_2$. Figure 6b shows the $^1O_2$ spectra under excitation of 980 nm (black curve) and under excitation of 540 nm (red curve). To the best of our knowledge, this is the first time of detecting $^1O_2$ photoluminescence from NIR-stimulated UCNPs, which confirms the highly efficient $^1O_2$ generation of NaYF$_4$:Yb^{3+},Er^{3+}—RB nanoconjugates.

Cancer Cell Imaging and Photodynamic Therapy. The targeting molecule, folic acid (FA), was covalently functionalized to NaYF$_4$:Yb^{3+},Er^{3+}—RB nanoconjugates *via* a dual functional PEG (NH$_2$—PEG—COOH). The reason for selecting PEG as linkers was twofold. On one hand, PEG has good compatibility to biological system, which can reduce the undesired toxicity of nanoparticles to normal tissue. On the other hand, tailoring folic acid at the end of the long chain of a PEG molecule can reduce steric hindrance for FA binding with its receptor and improve the targeting efficacy in cancer cells.

Figure 7 shows the target staining of the NaYF$_4$:Yb^{3+},Er^{3+}—RB/FA nanoplatform in JAR choriocarcinoma

TABLE 1. Fitting Parameters of Upconversion Luminescence Kinetics of NaYF$_4$:Yb^{3+},Er^{3+} and NaYF$_4$:Yb^{3+}, Er^{3+}—RB Conjugates with Triexponential Functions^a

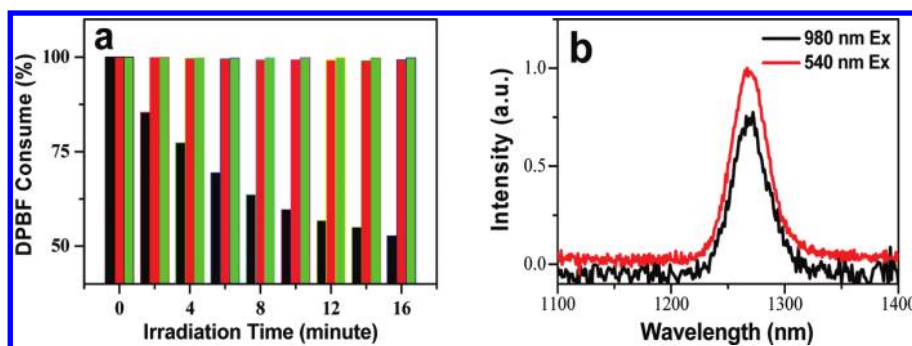|	NaYF$_4$:Yb^{3+},Er^{3+}			NaYF$_4$:Yb^{3+},Er^{3+}—RB		
	τ_{rise} (μs)	τ_{1decay} (μs)	τ_{2decay} (μs)	τ_{rise} (μs)	τ_{1decay} (μs)	τ_{2decay} (μs)
540 nm	5.37	82.15	177.92	4.28	51.90	164.01
650 nm	21.62	181.42	442.70	18.69	175.49	431.12
587 nm				2.74	43.70	

^{a} The instrumental response time is 10 ns.

Figure 6. $^1O_2$ is generated from UCNPs—PS nanoconjugates. (a) Consumption of DPBF over time (black); others were control experiments without UCNPs (red) or NIR (green). (b) $^1O_2$ luminescence spectra under excitation of 980 nm (in black) or 540 nm (in red).

cells and the control result using noncancerous NIH 3T3 cells. The fluorescence was collected at 650 nm from $NaYF_4:Yb^{3+},Er^{3+}$. The nanoconjugates were mainly located in cytoplasm and perinuclear regions (Figure 7, top), illustrating the endocytosis of the UCNP nanoplatform mediated by a folate receptor. On the contrary, when the folate receptors on a cancer cell membrane were saturated by free folic acid before incubating with the UCNP nanoplatform, few $NaYF_4:Yb^{3+},Er^{3+}-RB/FA$ nanoconjugates were stained in the cancer cells (Figure 7, middle), which might be due to the nonspecific adsorption of UCNPs. Furthermore, there was no significant morphology change observed in the cancer cells, suggesting the good biocompatibility of the $NaYF_4:Yb^{3+},Er^{3+}-RB/FA$ nanoplatform. To further verify the specificity of the UCNPs−RB conjugates, noncancerous NIH 3T3 cells, which are poor in expressing folate receptor, were used for a negative control (Figure 7, bottom), where only a few UCNPs were observed on the cells. All these results indicate the capability of using UCNPs−PS for targeted cancer cell imaging/diagnosis.

The photodynamic effect of UCNPs−PS nanoplatforms was studied by incubating JAR cells with UCNPs−PS at different concentrations. The cell viability determined

Figure 7. Specificity of the nanoconjugates. JAR carcinoma cells cultured in folate-free medium (top, positive) and in $100\times$ folate-supplemented medium (middle, negative). The negative control is also performed with NIH 3T3 cells (bottom).

from the 3-(4,5-dimethythiazol-2-yl)-2,5-diphenyl tetrazolium bromide (MTT) assay is shown in Figure 8. Dark toxicity, as a control, was also evaluated. No significant decrease in viability was observed in the control. It is known that RB has inherent concentration-dependent toxicity.[42] Our result shows that the toxicity becomes non-negligible only when its concentration is higher than 150 μg/mL (Figure S5), which is consistent with a previous report.[42] When JAR cancer cells were exposed to NIR light at a relatively low density of 1.5 W/cm^2, the cell viability decreased significantly with an increase in the concentration of UCNPs−PS conjugates, manifesting the feasibility of the nanoconjugates to decrease cancer cells. Compared with most previous reports in which much higher power density had to be used,[30] the covalently bonded UCNPs−PS nanoconjugates were obviously more efficient in killing cancer cells. As far as NIH 3T3 fibroblast cells are concerned, 980 nm irradiation had no obvious effect on cell viability, verifying the low expression of the nanoconjugates for the noncancerous cell line.

It is worth noting that the upconversion nanoplatform is restricted neither to $NaYF_4:Yb^{3+},Er^{3+}$ nanoparticles nor to RB. Since the upconversion emission spectrum is tunable in the UV/vis/NIR range, subject to dopant and/or host materials, the upconverted light for imaging can be tuned more to red to fall better into the optical window of tissues, when needed. In addition, selectable photosensitizers are expanded to the UV/vis range.

CONCLUSIONS

In conclusion, we have, employing a covalent bonding strategy, constructed a highly efficient NIR photosensitizing nanoplatform for simultaneous PDT and imaging. The covalent bonding between the $NaYF_4:Yb^{3+},Er^{3+}$ UCNPs and photosensitizers has significantly improved the quality of the nanoplatform. Compared with the generally adopted adsorption approach, both the photosensitizer loading capacity and the energy transfer efficiency from nanoparticles to photosensitizers have been significantly improved. The characteristic phosphorescence of $^1O_2$ at 1270 nm was readily detected for these photosensitizing nanoconjugates.

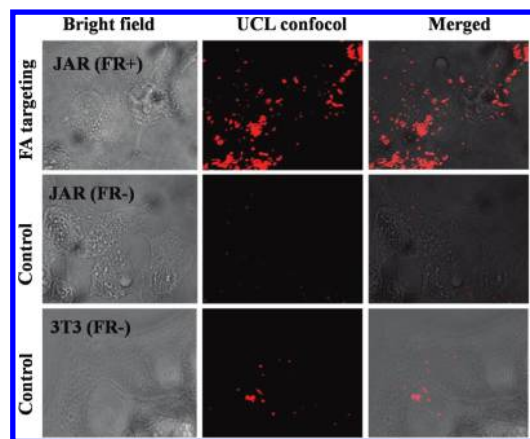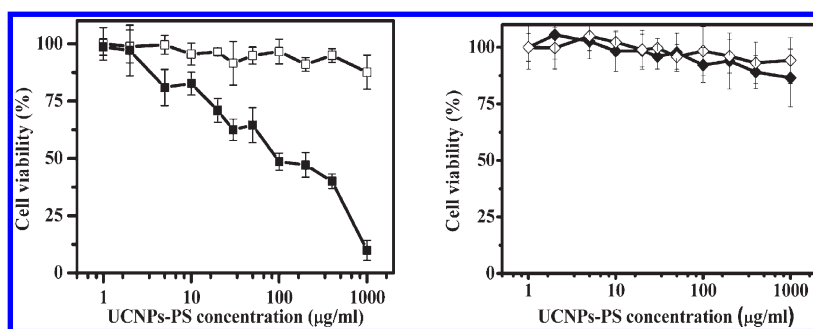**Figure 8. Viability of JAR cells (left) and NIH 3T3 fibroblasts (right)** treated with UCNPs−PS of different concentrations with (solid) or without (open) 980 nm exposure. Standard deviations are shown ($n = 5$).

The UCNPs–PS nanoplatforms have shown good biocompatibility and are able to perform fluorescence imaging and photodynamic therapy simultaneously under the same NIR light irradiation, highlighting the potential of these nanoplatforms in medical application.

EXPERIMENTAL METHODS

Synthesis of Amino-Functionalized NaYF$_4$:Yb^{3+},Er^{3+} UCNPs. Hexagonal-phase NaYF$_4$:Yb^{3+},Er^{3+} nanoparticles were synthesized by thermal decomposition of trifluoroacetate precursors in oleylamine following the earlier published methods.[43] In detail, 2 mmol of CF$_3$COONa, 0.78 mmol of (CF$_3$COO)$_3$Y, 0.2 mmol of (CF$_3$COO)$_3$Yb, and 0.02 mmol of (CF$_3$COO)$_3$Er (all from GFS Chemicals) were dissolved in 12 mL of oleylamine (Sigma Aldrich), and the mixture was heated to 120 °C for 1 h with vigorous magnetic stirring to remove water and oxygen under argon flow protection. The mixture was then heated to 320 °C for 1 h. After cooling to 80 °C, the produced nanoparticles were washed with ethanol at least three times, collected by centrifugation, and then dispersed in chloroform before further treatment.

In order to obtain amino-functionalized upconversion nanoparticles, a ligand exchange approach was adopted using 2-aminoethyl dihydrogenphosphate (AEP, Sigma Aldrich) to transform the hydrophobic NaYF$_4$:Yb^{3+},Er^{3+} nanoparticles into hydrophilic ones.[44] A 200 mg portion of AEP was first dispersed in 10 mL of a mixture of milli-Q water and ethanol with a volume ratio of 3:2, and then 5 mL of chloroform solution of OM-functioned NaYF$_4$:Yb^{3+},Er^{3+} nanoparticles (20 mg) was added dropwise into the AEP solution and stirred vigorously over 48 h at room temperature. Afterward, the UCNPs could be seen clearly transferred from the bottom chloroform layer into the top water layer under NIR excitation. After phase transfer, the NaYF$_4$:Yb^{3+},Er^{3+} nanoparticles were allowed to centrifuge and redispersed in 5 mL of water. The solution was stable for seven days without obvious aggregation.

Covalent Conjugation of NaYF$_4$:Yb^{3+},Er^{3+} UCNPs with Photosensitizers. The Rose Bengal hexanoic acid ester was obtained by reacting Rose Bengal (Sigma Aldrich) with hexanoic acid (Sigma Aldrich) and adopted for functionalization.[38] To covalently conjugate RB to UCNPs, 5 mL of dimethyl formamide (Sigma Aldrich) solution containing 2 mg of RB-HA, 20 mg of 1-ethyl-3-(3-dimethylaminopropyl)carbodiimide (Sigma Aldrich), and 20 mg of N-hydroxysulfosuccinimide sodium salt (Sigma Aldrich) was incubated at room temperature for 2 h, and then 10 mg of amino-functionalized NaYF$_4$:Yb^{3+},Er^{3+} upconversion nanoparticles was added into the solution and stirred vigorously for 24 h. UCNPs–PS conjugates were then centrifuged and washed with water to remove any unreacted RB. The amount of photosensitizer attached to UCNPs was calculated from the RB absorption spectrum.

To study further the stability of the covalently bonded UCNPs–PS conjugates, 2 mg of RB was also linked with 10 mg of UCNPs via electrostatic interaction and followed by the same washing procedure with water. Both conjugates formed via electrostatic and covalent bonding were then washed by DMSO, in which RB can dissolve well, followed by centrifugal separation. The process was repeated three times. The RB eluate was characterized by UV/vis absorption after each time separation. Using the RB eluate instead of the conjugates to study the stability was based on the fact that scattering of the conjugates was severe, which makes quantitative comparison difficult.

Singlet Oxygen Measurements. Two different methods were implemented to confirm the singlet oxygen generation, using the chemical probe DPBF or directly detecting its 1270 nm photoluminescence feature. In a typical DPBF experiment, 20 μL of a DPBF/ethanol solution (10 mmol/L) was added to 2 mL of a UCNPs–PS solution and transferred into a 10 mm cuvette. The solution was kept in the dark and irradiated with a 980 nm laser for 16 min, and the absorption intensity of DPBF at 417 nm was recorded every 2 min. For the control experiments, DPBF absorption was also recorded for comparison at the same conditions in the absence of UCNPs–PS or at 980 nm irradiation.

To detect the 1270 nm photoluminescence, UCNPs–PS nanoconjugates were collected by centrifugation, redispersed in D$_2$O, and then saturated with oxygen gas for 30 min before the experiment. Singlet oxygen production was measured under direct excitation of RB with 540 nm or indirect excitation of RB at 980 nm via FRET.

Target Cancer Cell Imaging and Therapy. In order to increase the specificity, folic acid was covalently linked with the NaYF$_4$:Yb^{3+}, Er^{3+} UCNPs in a similar way to RB cross-linking. FA–PEG ester was prepared using a heterobifunctional polyethylene glycol (COOH–PEG–NH$_2$, M_w = 3400, Nanocs) following the literature.[45,46] The FA–PEG was then mixed with 10 mg of UCNPs–PS and stirred for 24 h in the dark. The resulting nanoconjugates were collected by centrifugation, washed with water three times, redispersed in 5 mL of phosphate buffer, and stored in the dark at 4 °C for further application.

JAR choriocarcinoma cells that overexpress folate receptors (positive control) and NIH 3T3 fibroblasts that have a low expression of folate receptors (negative control) were purchased from American Type Culture Collection (ATCC). JAR cells were cultured in folate-free RPMI-1640 medium, and NIH 3T3 cells were cultured in DMEM medium. All the mediums were supplemented with 10% fetal bovine serum, 100 unit/mL penicillin, and 100 μg/mL streptomycin (all from Invitrogen). Cells were cultivated in medium at 37 °C in a humidified 95% air and 5% carbon dioxide (CO$_2$) atmosphere.

For confocal imaging, both JAR cells and NIH 3T3 cells were seeded on a coverslip at a concentration of 10^4 cells/mL and then treated with NaYF$_4$:Yb^{3+},Er^{3+}–RB/FA nanoconjugates (20 μg/mL) for 12 h at 37 °C. Prior to imaging, the coverslip was washed twice with phosphate-buffered saline (PBS) in order to remove any unbound upconversion nanoconjugates. To further study the specificity of the nanoconjugates, another negative control experiment was also carried out with JAR cells by supplementing 100 times more folic acid (100 mg/L) in the culture medium to saturate the folate receptors on the cell membrane before incubating with NaYF$_4$:Yb^{3+},Er^{3+}–RB/FA nanoconjugates.

To carry out photodynamic therapy of cancer cells, JAR cells were collected through centrifugation and diluted to a density of 1 × 10^5 cells/mL in the complete 1640 culture medium and then seeded onto 96-well plates (100 μL per well). After 24 h culturing, NaYF$_4$:Yb^{3+},Er^{3+}–RB/FA nanoconjugates were added to the culture medium at different concentrations from 0 to 1000 μg/mL, with five parallel wells for each concentration (0, 2, 5, 10, 20, 30, 50, 100, 200, 400, 1000 μg/mL). Before being exposed to NIR irradiation, the cells were allowed to incubate for another 24 h at 37 °C and then washed twice with PBS. A power-adjustable 980 nm fiber laser with maximal output power of 30 W (n-LIGHT Corporation) was collimated and employed as area light source to irradiate the 96-well plate. After 10 min exposure of 980 nm light at 1.5 W/cm^2, the cells were allowed to incubate for an additional 48 h. Cell viability was measured according to the standard MTT (Sigma Aldrich) assay method. Typically, 10 μL of MTT solution (5 mg/mL MTT in PBS, pH 7.4) was added to each well and incubated for 4 h at 37 °C. After removing the medium, the wells were washed by PBS, and then the intracellular formazan crystals were extracted into 100 μL of DMSO. The absorbance of cell lysate was recorded at 550 nm by a plate reader, and the cell viability could be calculated from the average value of five parallel wells.

The choice of exposure power density of 1.5 W/cm^2 was based on the following consideration. In clinical applications and most PDT experiments the light dose is in the range of

1–1000 J/cm^2, and the typical power density is below 1 W/cm^2.[47] But this value is obtained in the Stokes case, *i.e.*, direct excitation of photosensitizers, whereas in our case it is an anti-Stokes scheme, *i.e.*, indirect excitation (NIR light converted into UV/vis, and the latter is then used to excite the photosensitizers) where the efficiency is less than the direct excitation and the required excitation power density should be higher. However higher excitation power density may lead to thermal decline of the cells. In the current case the highest possible excitation power density was determined to be ~2 W/cm^2. Therefore 1.5 W/cm^2 was used in our study.

Instruments. Structure characterization was performed with TEM images obtained with a Morgagni transmission electron microscope (FEI Company). UV–vis spectra of solutions were recorded in quartz cuvettes (1 cm) with a Hewlett-Packard/ Agilent 8453 diode-array biochemical analysis UV–vis spectrophotometer. The steady-state upconversion luminescence spectra of UCNPs and UCNPs–PS nanoconjugates were detected using a Horiba Jobin Yvon Spex Fluorolog 3 spectrofluorometer. A CW semiconductor diode laser of 980 nm was used to excite the samples. To record the $^1O_2$ emission at 1270 nm, a high-sensitive liquid nitrogen cooled InGaAs detector (DSS-IGA020L) was coupled to the Spex spectrofluorometer. Time-resolved luminescence was measured with a Hamamatsu R9110 PMT in a single-photon counting setup.[48]

Wide field imaging and upconversion luminescent confocal imaging of cancer cells were carried out using an inverted Olympus IX71 microscope system equipped with an 100× oil immersion objective.[49] The 980 nm excitation light was from Ti: Sapphire laser Chameleon ULTRA-II (80 fs, 80 MHz), which was coupled to the adapted confocal unit. The emitted light was passed through a dichroic mirror and a 650 nm bandpass filter (fwhm: 10 nm) and recorded by CCD camera.

Conflict of Interest: The authors declare no competing financial interest.

REFERENCES AND NOTES

1. Castano, A. P.; Mroz, P.; Hamblin, M. R. Photodynamic Therapy and Anti-Tumour Immunity. *Nat. Rev. Cancer* **2006**, *6*, 535–545.

2. Braathen, L. R.; Szeimies, R. M.; Seguin, N. B.; Bissonnette, B.; Foley, P.; Pariser, D.; Roelandts, R.; Wennberg, A. M.; Morton, C. A. Guidelines on the Use of Photodynamic Therapy for Nonmelanoma Skin Cancer: An International Consensus. *J. Am. Acad. Dermatol.* **2007**, *56*, 125–143.

3. Wolf, P.; Rieger, E.; Kerl, H. Topical Photodynamic Therapy with Endogenous Porphyrins After Application of 5-Aminolevulinic Acid: An Alternative Treatment Modality for Solar Keratoses, Superficial Squamous Cell Carcinomas, and Basal Cell Carcinomas? *J. Am. Acad. Dermatol.* **1993**, *28*, 17–21.

4. Celli, J. P.; Spring, B. Q.; Rizvi, I.; Evans, C. L.; Samkoe, K. S.; Verma, S.; Pogue, B. W.; Hasan, T. Imaging and Photodynamic Therapy: Mechanisms, Monitoring, and Optimization. *Chem. Rev.* **2010**, *12*, 2795–838.

5. O'Brien, T.; Thomas, K. Bladder Cancer: Photodynamic Diagnosis Can Improve Surgical Outcome. *Nat. Rev. Urol.* **2010**, *7*, 598–599.

6. Rai, P.; Mallidi, S.; Zheng, X.; Rahmanzadeh, R.; Mir, Y.; Elrington, S.; Khurshid, A.; Hasan, T. Development and Applications of Photo-Triggered Theranostic Agents. *Adv. Drug Delivery Rev.* **2010**, *62*, 1094–1124.

7. Fritsch, C.; Lang, K.; Neuse, W.; Ruzicka, T.; Lehman, P. Photodynamic Diagnosis and Therapy in Dermatolog. *Skin Pharmacol. Appl. Skin Physiol.* **1998**, *11*, 358–373.

8. Chatterjee, D. K.; Rufaihah, A. J.; Zhang, Y. Upconversion Fluorescence Imaging of Cells and Small Animals Using Lanthanide Doped Nanocrystals. *Biomaterials* **2008**, *29*, 937–943.

9. Wang, M.; Mi, C. C.; Wang, W. X.; Liu, C. H.; Wu, Y. F.; Xu, Z. R.; Mao, C. B.; Xu, S. K. Immunolabeling and NIR-Excited Fluorescent Imaging of Hela Cells by Using NaYF4: Yb^{3+}, Er^{3+} Upconversion Nanoparticles. *ACS Nano* **2009**, *3*, 1580–1586.

10. Idris, N. M.; Li, Z.; Ye, L.; Sim, E. K.; Mahendran, R.; Ho, P. C. L.; Zhang, Y. Tracking Transplanted Cells in Live Animal Using Upconversion Fluorescent Nanoparticles. *Biomaterials* **2009**, *30*, 5104–5113.

11. Xiong, L. Q.; Chen, Z. G.; Yu, M. X.; Li, F. Y.; Liu, C.; Huang, C. H. Synthesis, Characterization, and In Vivo Targeted Imaging of Amine-Functionalized Rare-Earth Up-Converting Nanophosphors. *Biomaterials* **2009**, *30*, 5592–5600.

12. Yu, X. F.; Sun, Z.; Li, M.; Xiang, Y.; Wang, Q. Q.; Tang, F.; Wu, Y.; Cao, Z.; Li, W. Neurotoxin Conjugated Upconversion Nanoprobes for Direct Visualization of Tumors under Near-Infrared Irradiation. *Biomaterials* **2010**, *31*, 8724–8731.

13. Zako, T.; Nagata, H.; Terada, N.; Utsumi, A.; Sakono, M.; Yohda, M.; Ueda, H.; Soga, K.; Maeda, M. Cyclic RGD Peptide-Labeled Upconversion Nanophosphors for Tumor Cell Targeted Imaging. *Biochem. Biophys. Res. Commun.* **2009**, *381*, 54–58.

14. Chen, Q.; Wang, X.; Chen, F.; Zhang, Q.; Dong, B.; Yang, H.; Liu, G.; Zhu, Y. Functionalization of Upconverted Luminescent NaYF4: Yb/Er Nanocrystals by Folic Acid Chitosan Conjugates for Targeted Lung Cancer Cell Imaging. *J. Mater. Chem.* **2011**, *21*, 7661–7667.

15. Hilderbrand, S. A.; Shao, F. W.; Salthouse, C.; Mahmood, U.; Weissleder, R. Upconverting Luminescent Nanomaterials: Application to In Vivo Bioimaging. *Chem. Commun.* **2009**, *28*, 4188–4190.

16. Zhou, J.; Sun, Y.; Du, X. X.; Xiong, L. Q.; Hu, H.; Li, F. Y. Dual-Modality In Vivo Imaging Using Rare-Earth Nanocrystals with Near-Infrared to Near-Infrared (NIR-to-NIR) Upconversion Luminescence and Magnetic Resonance Properties. *Biomaterials* **2010**, *31*, 3287–3295.

17. Kobayashi, H.; Kosaka, N.; Ogawa, M.; Morgan, N. Y.; Smith, P. D.; Murray, C. B.; Ye, X. C.; Collins, J.; Kumar, G. A.; Bell, H.; *et al.* In Vivo Multiple Color Lymphatic Imaging Using Upconverting Nanocrystals. *J. Mater. Chem.* **2009**, *19*, 6481–6484.

18. Xiong, L. Q.; Chen, Z. G.; Tian, Q. W.; Cao, T. Y.; Xu, C. J.; Li, F. Y. High Contrast Upconversion Luminescence Targeted Imaging In Vivo Using Peptide-Labeled Nanophosphors. *Anal. Chem.* **2009**, *81*, 8687–8694.

19. Cheng, L.; Yang, K.; Zhang, S.; Shao, M. W.; Lee, S.; Liu, Z. Highly Sensitive Multiplexed In Vivo Imaging Using PEGylated Upconversion Nanoparticles. *Nano Res.* **2010**, *3*, 722–732.

20. Nyk, M.; Kumar, R.; Ohulchanskyy, T. Y.; Bergey, E. J.; Prasad, P. N. High Contrast In Vitro and In Vivo Photoluminescence Bioimaging Using Near Infrared to Near Infrared Up-Conversion in Tm^{3+} and Yb^{3+} Doped Fluoride Nanophosphors. *Nano Lett.* **2008**, *8*, 3834–3838.

21. Park, Y.; Kim, J. H.; Lee, K. T.; Jeon, K. S.; Na, H. B.; Yu, J. H.; Kim, H. M.; Lee, N.; Choi, S. H.; Baik, S.; *et al.* Nonblinking and Nonbleaching Upconverting Nanoparticles as an Optical Imaging Nanoprobe and T1Magnetic Resonance Imaging Contrast. *Adv. Mater.* **2009**, *21*, 4467–4471.

22. Wang, C.; Cheng, L.; Liu, Z. Drug Delivery with Upconversion Nanoparticles for Multi-functional Targeted Cancer Cell Imaging and Therapy. *Biomaterials* **2011**, 1110–1120.

23. Zhou, J.; Yu, M. X.; Sun, Y.; Zhang, X. Z.; Zhu, X. J.; Wu, Z. H.; Wu, D. M.; Li, F. Y. Fluorine-18-Labeled Gd^{3+}/Yb^{3+}/Er^{3+} Co-doped NaYF$_4$ Nanophosphors for Multimodality PET/MR/UCL Imaging. *Biomaterials* **2011**, *32*, 1148–1156.

24. Yang, Y. M.; Shao, Q.; Deng, R. R.; Wang, C.; Teng, X.; Cheng, K.; Cheng, Z.; Huang, L.; Liu, Z.; Liu, X. G.; *et al.* In Vitro and

In Vivo Uncaging and Bioluminescence Imaging by Using Photocaged Upconversion Nanoparticles. *Angew. Chem., Int. Ed.* **2012**, *51*, 1–6.

25. Cheng, L.; Yang, K.; Li, Y. G.; Zeng, X.; Shao, M. W.; Lee, S. T.; Liu, Z. Multifunctional Nnoparticles for Upconversion Luminescence/MR Multimodal Imaging and Magnetically Targeted Photothermal Therapy. *Biomaterials* **2012**, *33*, 2215–2222.

26. Zhou, J.; Liu, Z.; Li, F. Y. Upconversion Nanophosphors for Small-Animal Imaging. *Chem. Soc. Rev.* **2012**, *41*, 1323–1349.

27. Zhang, P.; Steelant, P.; Kumar, M.; Scholfield, M. Versatile Photodynamic Therapy at Infrared Excitation. *J. Am. Chem. Soc.* **2007**, *129*, 4526–4527.

28. Qian, H. S.; Guo, H. C.; Ho, P. C.; Mahendran, R.; Zhang, Y. Mesoporous-Silica-Coated Up-Conversion Fluorescent Nanoparticles for Photodynamic Therapy. *Small* **2009**, *5*, 2285–2290.

29. Guo, H. C.; Qian, H. S.; Idris, N. M.; Zhang, Y. Singlet Oxygen-induced Apoptosis of Cancer Cells Using Upconversion Fluorescent Nanoparticles as a Carrier of Photosensitizer. *Nanomedicine: NBM* **2010**, *6*, 486–495.

30. Shan, J. N.; Budijono, S. J.; Hu, G. H.; Yao, N.; Kang, Y. B.; Ju, Y. G.; Prud'homme, R. K. Pegylated Composite Nanoparticles Containing Upconverting Phosphors and meso-Tetraphenylporphine (TPP) for Photodynamic Therapy. *Adv. Funct. Mater.* **2011**, *21*, 2488–2495.

31. Wang, C.; Tao, H. Q.; Cheng, L.; Liu, Z. Near-Infrared Light Induced *In Vivo* Photodynamic Therapy of Cancer Based On Upconversion Nanoparticles. *Biomaterials* **2011**, *32*, 6145–6154.

32. Lim, M. E.; Lee, Y. L.; Zhang, Y.; Chu, J. J. H. Photodynamic Inactivation of Viruses Using Upconversion Nanoparticles. *Biomaterials* **2012**, *33*, 1912–1920.

33. Chatterjee, D. K; Zhang, Y. Upconverting Nanoparticles As Nanotransducers for Photodynamic Therapy in Cancer Cells. *Nanomedicine* **2008**, *3*, 73–82.

34. Zhang, F.; Ying Wan, Y.; Yu, T.; Zhang, F. Q.; Shi, Y. F.; Xie, S. H.; Li, Y. G.; Xu, L.; Tu, B.; Zhao, D. Y. Uniform Nanostructured Arrays of Sodium Rare-Earth Fluorides for Highly Efficient Multicolor Upconversion Luminescence. *Angew. Chem., Int. Ed.* **2007**, *46*, 7976–7979.

35. Wang, F.; Liu, X. G. Upconversion Multicolor Fine-Tuning Visible to Near Infrared Emission from Lanthanide-Doped $NaYF_4$ Nanoparticles. *J. Am. Chem. Soc.* **2008**, *130*, 5642–5643.

36. Myller, A. T; Karhe, J. J.; Pakkanen, T .T. Preparation of Amino Functionalized TiO_2 Surfaces by Binding of Organophosphates. *Appl. Surf. Sci.* **2010**, *257*, 1616–1622.

37. Tanielian, C.; Schweitzer, C.; Mechin, R.; Wolff, C. Quantum Yield of Singlet Oxygen Production by Monomeric and Aggregated Forms of Hematoporphyrin Derivative. *Free Radicals Biol. Med.* **2001**, *30*, 208–212.

38. Lamberts, J. J. M.; Schumacher, D. R.; Neckers, D. C. Novel Rose Bengal Derivatives: Synthesis and Quantum Yield Studies. *J. Am. Chem. Soc.* **1984**, *106*, 5879–5883.

39. Jiang, S; Zhang, Y. Upconversion Nanoparticle-Based FRET System for Study of siRNA. *Langmuir* **2010**, *26*, 6689–6694.

40. Wang, Y.; Liu, K.; Liu, X. M.; Dohnalova, K.; Gregorkiewicz, T.; Kong, X. G.; Aalders, M. C. G.; Buma, W. J.; Zhang, H. Critical Shell Thickness of Core/Shell Upconversion Luminescence Nanoplatform for FRET Application. *J. Phys. Chem. Lett.* **2011**, *2*, 2083–2088.

41. Tang, W.; Xu, H.; Kopelman, R.; Philbert, M. A. Photodynamic Characterization and *In Vitro* Application of Methylene Blue-containing Nanoparticle Platforms. *Photochem. Photobiol.* **2005**, *81*, 242–249.

42. Mousavi, S. H.; Afshari, J. T.; Brook, A.; Anarkooli, I. J. Direct Toxicity of Rose Bengal in MCF-7 Cell Line: Role of Apoptosis. *Food Chem. Toxicol.* **2009**, *47*, 855–859.

43. Wang, Y.; Tu, L. P.; Zhao, J. W.; Sun, Y. J.; Kong, G. K.; Zhang, H. Upconversion Luminescence of β-NaYF4: Yb^{3+}, Er^{3+}@β-NaYF4 Core/Shell Nanoparticles: Excitation Power Density and Surface Dependence. *J. Phys. Chem. C* **2009**, *113*, 7164–7169.

44. Song, K.; Kong, X. G.; Liu, X. M.; Zhang, Y. L.; Zeng, Q. H.; Tu, L. P.; Shi, Z.; Zhang, H. Aptamer Optical Biosensor Without Bio-breakage Using Upconversion Nanoparticles as Donors. *Chem. Commun.* **2012**, *48*, 1156–1158.

45. Low, P. S.; Henne, W. A.; Doorneweerd, D. D. Discovery and Development of Folic-Acid-Based Receptor Targeting for Imaging and Therapy of CancerandInflammatory Diseases. *Acc. Chem. Res.* **2008**, *41*, 120–129.

46. Zhang, C.; Gao, S. J.; Jiang, W.; Lin, S.; Du, F. S.; Li, Z. C.; Huang, W. L. Targeted Minicircle DNA Delivery Using Folate-Poly(ethylene glycol)-Polyethylenimine As Non-Viral Carrier. *Biomaterials* **2010**, *31*, 6075–6086.

47. Niemz, M. H. *Laser-Tissue Interactions: Fundamentals and Applications*, 3rd ed.; Springer: Heidelberg, 2007; pp 45−58.

48. Boer, W. D. A. M.; Timmerman, D.; Dohnalová, K.; Yassievich, I. N.; Zhang, H.; Buma, W. J.; Gregorkiewicz, T. Red Spectral Shift and Enhanced Quantum Efficiency in Phonon-Free Photoluminescence from Silicon Nanocrystals. *Nat. Nanotechnol.* **2010**, *5*, 878–884.

49. Siekierzycka, J. R.; Catharina Hippius, C.; Würthner, F.; Williams, R. M.; Brouwer, A. M. Polymer Glass Transitions Switch Electron Transfer in Individual Molecules. *J. Am. Chem. Soc.* **2010**, *132*, 1240–1242.